PHYSICAL REVIEW B VOLUME 47, NUMBER 7 15 FEBRUARY 1993-I

Hubbard model at infinite dimensions: Thermodynamic and transport properties

Th. Pruschke and D. L. Cox
Department of Physics, The Ohio State University, Columbus, Ohio 43210-1106

M. Jarrell
Department of Physics, University of Cincinnati, Cincinnati, Ohio 45221-0011
(Received 11 August 1992)

We present results on the thermodynamic quantities, resistivity, and optical conductivity for the Hubbard model on a simple hypercubic lattice in infinite dimensions. Our results for the paramagnetic phase display the features expected from an intuitive analysis of the one-particle spectra and substantiate the similarity of the physics of the Hubbard model to those of heavy-fermion systems. The calculations were performed using an approximate solution to the single-impurity Anderson model, which is the key quantity entering the solution of the Hubbard model in this limit. To establish the quality of this approximation we compare its results, together with those obtained from two other widely used methods, to essentially exact quantum Monte Carlo results.

I. INTRODUCTION

The limit of infinite spatial dimensions has turned out to be a natural starting point for obtaining sensible approximate[1–4], and even essentially exact[5,6] solutions of models of highly correlated electronic systems. In this limit the dynamics of the system become essentially local[3] which considerably simplifies the task of calculating quantities of interest[2,5–7].

In the present paper we want to extend our previous study of the Hubbard Hamiltonian[5,6,8]

$$H = \sum_{\langle ij\rangle,\sigma} t_{ij}\left(c^{\dagger}_{i,\sigma}c_{j,\sigma} + \text{H.c.}\right) - \mu\sum_{i\sigma} n_{i\sigma} + U\sum_{i} n_{i,\uparrow}n_{i,\downarrow} \quad (1)$$

in the limit of infinite spatial dimensions $d = \infty$. The notation in (1) is the standard one and the limit $d \to \infty$ has to be taken such that $t^{*2} \equiv d\langle t^2_{\mathbf{k}}\rangle_{\mathbf{k}} = \text{const}$. Based on observations made by Brandt and Mielsch[2], several groups[5–7] independently demonstrated that the one-particle Green's function, or equivalently the proper one-particle self-energy of the model (1), in this limit is obtained from the equation

$$G_{ii}(z) = \int d\omega\, A_0(\omega)\frac{1}{z-\omega-\epsilon-\Sigma(z)} = \mathcal{G}(z)\,. \quad (2)$$

Here, the Green's function $\mathcal{G}(z)$ is the solution of a single-impurity Anderson model with an effective hybridization given by[6]

$$\Delta(z) = \frac{1}{G_{ii}(z)} + \Sigma(z) - z - \mu \quad (3)$$

and $A_0(\epsilon)$ denotes the free one-particle density of states (DOS). Note that for a given site i Eq. (3) defines an effective potential due to the presence of the lattice. Equations (2) and (3) thus constitute the "natural" mean-field theory for the Hubbard model (1)[4].

This mean-field theory is of course independent of the lattice structure. For reasons of convenience, however, we shall concentrate on a simple hypercubic lattice with N sites and transfer along the d-coordinate axes only, i.e., $t_{\mathbf{k}} = -2\sum_{m=1}^{\infty} t_m \sum_{n=1}^{d}\cos(mk_n)$. The latter assumption obviously oversimplifies the situation when one wants to consider transfer beyond nearest neighbors, but it has the advantage that the free single-particle DOS

$$A_0(\epsilon) = \frac{1}{N}\sum_{\mathbf{k}}\delta(\epsilon - t_{\mathbf{k}}) \quad (4)$$

acquires the simple Gaussian form[3]

$$A_0(\epsilon) = \exp(-\epsilon^2)/\sqrt{\pi} \quad (5)$$

when $t^{*2} = \sum t^{*2}_m = 1$. The latter convention will set the energy scale used for the remainder of this paper. For nearest-neighbor transfer and $\mathbf{q} = (\pi, \pi, \ldots)$ one has perfect nesting. However, any $t_2 \neq 0$ destroys this property and thus allows us to continuously bias quantities which depend on the perfect nesting like magnetic instabilities.

The situation with nearest-neighbor transfer only was explored in Refs. 5 and 6 using a quantum Monte Carlo (QMC) method to solve the impurity Anderson model. We could thus obtain essentially exact results for the model (1) and discuss magnetic and single-particle properties for a variety of model parameters and temperatures. The results at half filling $n_e = 1$ can most conveniently be presented in the phase diagram in Fig. 1: For small values of U and high temperatures one finds a paramagnetic metal with correlation-enhanced Fermi-liquid parameters. By increasing U for a fixed temperature a crossover through a semimetalliclike (shaded region) into a Mott-Hubbard-like phase with exponentially reduced DOS at μ takes place. Note that one never finds a true gap in the DOS for this "phase." Nevertheless, transport and thermodynamic properties will essentially behave like an insulator. By lowering the temperature for fixed U, one encounters an antiferromagnetic transition which is connected with a gap in the one-particle

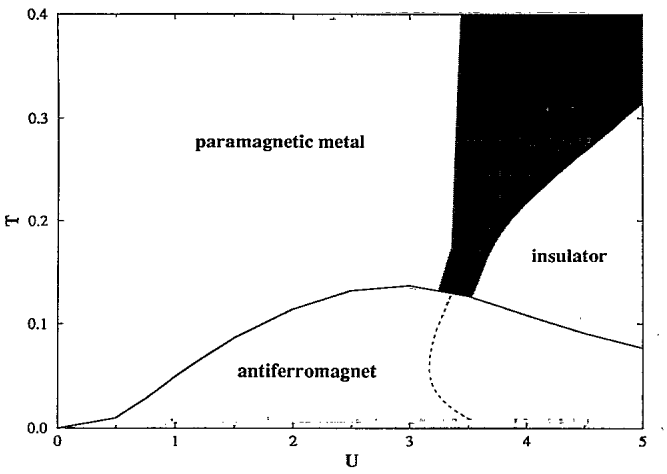

FIG. 1. Phase diagram of the infinite-dimensional Hubbard model at half filling. The shaded region is a rough estimate of the crossover region where the physics of the system resembles that of semimetal with thermally induced DOS at μ. Beyond this region it essentially behaves like an insulator.

DOS due to the cell doubling associated with the antiferromagnetic state. As mentioned earlier, this phase can be shifted to lower temperatures or even be completely suppressed by magnetically frustrating the system by a finite t_2. In this case the dotted line in the antiferromagnetic region in Fig. 1 becomes important. It visualizes the behavior of the metal-insulator (MI) crossover for a fixed U when the temperature is lowered and shows an interesting and unexpected reentrance behavior. As we will discuss later, this is connected to a competition between the "Mott-Hubbard" phase and the Kondo effect also present in this model[6].

This Kondo effect is apparent as the temperature approaches some small-energy scale. There are two ways we may define such an energy scale. First, we can obtain an "effective impurity" Kondo scale T_K from the self-consistently embedded impurity by calculating the screened local moment on the site i, $T\chi(T)_{ii}$, and then extracting T_K by fitting this result to the universal numerical renormalization-group results of Krishnamurthy, Wilkens, and Wilson[9]. We find that T_K defined in this way is strongly temperature dependent, increasing with decreasing T (Ref. 6). This temperature dependence of T_K can easily be understood—and is, in fact, expected—from the obvious temperature dependence of the effective medium defined by (3). It also explains the observed rather fast disappearance of the Abrikosov-Suhl resonance (ASR) in the one-particle DOS, associated with this Kondo screening, with increasing temperature and its total absence in the semimetallic region of the phase diagram. Second, we may also identify a scale T_0 as where the ASR in the density of states reaches half its maximum value. This latter energy scale appears to be more physically meaningful since it shows up in physical quantities like specific heat and resistivity.

Away from half filling the Mott-Hubbard phase is immediately replaced by a Fermi liquid with strongly enhanced Fermi-liquid parameters. More precisely, we found a narrow resonance at μ for low temperatures which leads to the observed enhanced quasiparticle mass. This resonance could again be traced to a Kondo screening of the local moments with a dynamically generated low-temperature energy scale—T_0—connected to it. The magnetic transition is also found to be suppressed upon doping. Finally, for greater than 20% doping, correlation effects become less important and the system basically behaves like one would expect from standard perturbation theory.

The remainder of this paper is split into three parts. First, we will compare different approximation schemes to the QMC results. The main reason is that QMC is rather time intensive and becomes problematic for large values of U and inverse temperature β. Also, by virtue of the method, the QMC process gives all dynamical quantities as a function of Matsubara rather than real frequency and one has to use, e.g., maximum entropy methods to analytically continue these results to real frequencies. Although this is straightforward for densities of states, it proves problematic for quantities like the one-particle self-energy. On the other hand, several physical quantities need this real-frequency dependence as input. As we will show, a good approximation scheme for this purpose is given by a self-consistent perturbation theory developed for the single-impurity Anderson model (NCA)[10,11]. In the second part of the paper we use this approximation to calculate free energy, specific heat, resistivity, and optical conductivity for the model (1) for the paramagnetic phase. Finally, a discussion will close the paper.

II. COMPARISON OF DIFFERENT METHODS

One major problem in using the QMC approach to calculate physical quantities is the rather large amount of computer time one has to invest to obtain results for one particular set of parameters. Especially for thermodynamic properties, where one has to adjust the chemical potential to maintain a fixed filling, it is difficult to calculate a temperature series. It is thus clearly desirable to have some different methods to solve the Hamiltonian (1) or, equivalently, the single-impurity Anderson model.

The most straightforward idea is to use standard perturbation theory in U. This is known to work rather well for the symmetric single-impurity Anderson model[12,13], and one thus may expect it to be a reasonable approximation at half filling and for small values of U. Away from the symmetric point it is known that at least the lowest order does not reproduce the correct occupation number[7]. Nevertheless, it is a simple method and it is surely worthwhile to outline its region of applicability. It also has the advantage that it automatically fulfills Fermi-liquid sum rules. A rather complete discussion up to second order in U has been reported by Menge and Müller-Hartmann[14,15]. Since it has been pointed out by Georges and Kotliar[7] that these results are not qualitatively much different from the lowest second-order result with Hartree self-consistency[13,16], we shall use the latter approach here.

The most successful approximate methods for dealing with highly correlated electron systems have been developed for the single-impurity Anderson model by choosing the mixing term as perturbation[17]. Unfortunately, the price one has to pay for leaving the Coulomb interaction intact is that the standard methods of perturbation theory fail. This problem can be nicely circumvented for the impurity problem, leading to well-defined and controlled approximation schemes like the so-called NCA (Refs. 10, 11, and 17). This approximation is known to work well when the physics of the system is dominated by spin fluctuations[18,19] but fails when charge excitations become important. In this respect it may be viewed as an approach complementary to standard perturbation theory. In addition, the NCA tends to violate Fermi-liquid properties for temperatures much lower than the smallest energy scale in the problem[19]. However, the NCA is nevertheless quite reliable over a large interval of parameters including temperature[10]. Since the solution of the model (1) for $d = \infty$ essentially reduces to the solution of a single-impurity Anderson model it is natural to adopt the NCA for this problem.

Another natural attempt is to extend the perturbation theory with respect to mixing directly onto concentrated systems. In this case, however, the missing features of standard perturbation theory complicate the problem considerably[20] and a controlled approximation (like in the impurity case) presently does not exist. With the use of some *ad hoc* assumptions it is nevertheless possible to set up an approximation for this problem, too. These theories are originally designed for the periodic Anderson model and are known in the literature as XNCA (Ref. 21) and LNCA (Refs. 22 and 23). Recently, one of the authors has shown that any such theory for the periodic Anderson model can be readily employed for the Hubbard model (1), too[24,25]. In order to obtain an idea about the quality of these approximations we include the LNCA in our comparison.

The single-particle density of states for the Hubbard model (1) at half filling $n = 1$ for several values of U at an inverse temperature $\beta = 7.2$ is shown in Fig. 2 for the different kind of approaches discussed before. Let us first outline the general features of the DOS as they appear from the QMC results: In all cases one finds two prominent peaks at roughly $\pm U/2$ which have to be identified with charge excitations on and off the local levels. In addition there is a pronounced resonance at μ for small values of U due to coherent movement of the particles in the system. This feature is suppressed when U is increased and eventually a pseudogap opens at μ.

In comparing the different approximations to the QMC results the first thing to note is that the overall agreement between QMC and NCA, apart from small differences at μ, is very good. For $U = 6$ we did not succeed in analytically continuing the QMC results. The only quantity we were able to obtain here is the position of the edges of the pseudogap. These were found to be in good agreement with those predicted by the NCA. We want to point out that for this value of U, as generally for values U well inside the "insulator" phase in Fig. 1 and $\beta U \gg 1$, the NCA does not provide stable results but tends to produce

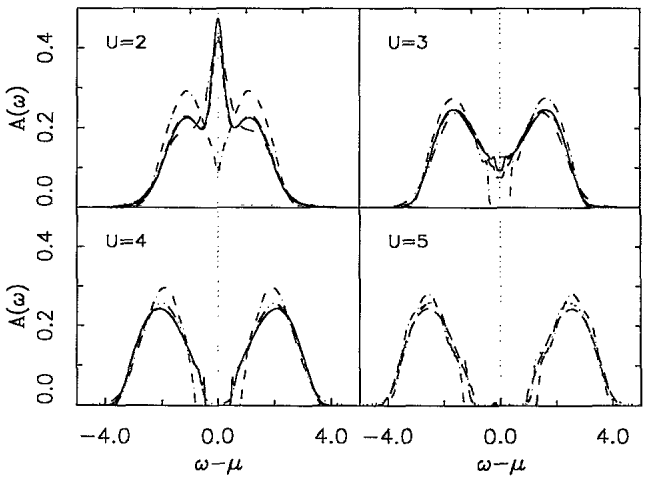

FIG. 2. DOS for the Hubbard model at half filling and $\beta = 7.2$ for some values of U. The full line represents the QMC result, the dashed line the NCA, the dashed-dotted line the LNCA, and the results obtained from perturbation theory are given by the dotted-dashed-dotted line. No QMC results are available for $U = 5$.

spurious oscillations at the gap edges. However, general structures like the width of the pseudogap are reproduced with good accuracy. Nevertheless, these instabilities prohibit a thorough investigation of this surely very interesting part of the phase diagram at half filling. We want to emphasize that this problem *is not intrinsic to the NCA*, but rather must be attributed to numerical instabilities of the computer code used to solve the NCA equations. The reason is that structures in the NCA equations become very sharp in this region and eventually cannot be resolved on a discrete energy mesh. When this occurs we approximate these structures as poles, which gives rise to the mentioned numerical instabilities. Note that this problem does not occur outside the insulator phase and off-half filling. A rather interesting point is that "poles" in the NCA begin to develop exactly when the DOS at μ becomes exponentially small. This empirical observation was also confirmed by QMC for some characteristic points in the phase diagram and eventually used to find an estimate of the right-hand border of the crossover region in Fig. 1.

Apparently, at half filling perturbation theory in U generally reproduces qualitatively both the high- and the low-energy features of the DOS. The LNCA, on the other hand, looks like a too large value of U had been used. This may be attributed to the approximations involved which put a strong emphasis on local correlations and are thus likely to overestimate residual local interactions. It also clearly overestimates the charge excitation bands and shows little of the finer structure near the gap edges[6], but at least it reproduces the general features of the DOS qualitatively correctly and accounts for the existence of the pseudogap.

In Fig. 3 we present some typical results off half filling, namely for $\mu = 1$ ($n_e \approx 0.94$) and $\mu = 0.5$ ($n_e \approx 0.8$) at two different temperatures $\beta = 3.6$ and $\beta = 14.4$. The value of the Coulomb repulsion is $U = 4$. Again, QMC

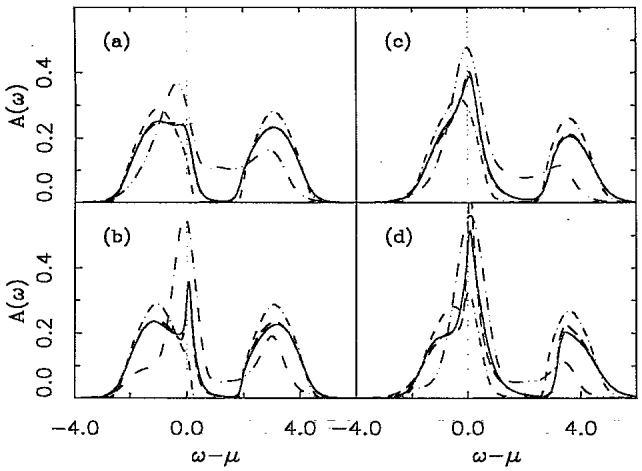

FIG. 3. DOS for two typical fillings $n_e < 1$ and different temperatures at a $U = 4$. (a) and (b) show $\mu = 1$ ($n_e \approx 0.94$) for $\beta = 3.6$ and 14.4, respectively, while (c) and (d) collect results for $\mu = 0.5$ ($n_e \approx 0.8$) at the same temperatures. The line patterns are the same as in Fig. 2.

and NCA are in good agreement concerning the high- and the low-energy features except for Fig. 3(d), where $A_{\mathrm{NCA}}(\mu)$ comes out much too large, i.e., the NCA fails to account properly for the low-energy physics. This is the principal failure directly related to the approximations involved in the NCA (Ref. 19).

Interestingly, the LNCA gives a much weaker temperature dependence of the DOS at μ, indicating that this approximation underestimates the characteristic low-energy scale T_0. This is in accordance with the observation made earlier, namely that the LNCA tends to overestimate the role of the local correlations. Apart from this failure the general form of the spectra agrees at least qualitatively with the exact result. To obtain reasonable results from perturbation theory, we found it necessary to fix the occupancy to the QMC value by adjusting the chemical potential. This given, the perturbation theory apparently becomes better with increasing hole concentration. It nevertheless produces features which are too broad and rather poor imitations of the charge excitation peaks.

A first conclusion one may draw from these considerations is that the NCA reproduces most of the general features of the single-particle DOS with good accuracy. However, Fig. 3(d) clearly shows that for some choice of parameter values the most important region at μ is approximated very poorly. In order to achieve a better classification of the portion of the parameter space where the NCA constitutes a reliable approximation to the problem, let us substantiate the differences between QMC and NCA by looking at the quasiparticle weight defined by

$$\zeta^{-1}(T) = 1 - \frac{\mathrm{Im}\Sigma(i\omega_0)}{\omega_0} \quad , \tag{6}$$

where $\omega_0 = \pi T$ is the lowest Matsubara frequency[26]. Figure 4 displays this function for $\mu = 1$ and $U = 4$ as obtained from QMC (circles) and NCA (squares). Note that for these parameter values we expect $T_0 \approx 1/8$ (Ref. 6), i.e., $\zeta^{-1}(T \to 0) \approx 8$. The agreement between QMC and NCA is satisfactory, especially for temperatures $T \gtrsim T_0/2$. For temperatures $T \lesssim T_0/2$ the values obtained by the NCA become too large although the order of magnitude is still good. Things become worse as soon as $T \ll T_0$, where the NCA produces again an upturn instead of a saturation. Both the slightly too large values as well as the failure for $T \lesssim T_0/5$ must be attributed to the well-known pathology of the NCA (Ref. 19). In our case, the most important aspect of this pathology is its tendency to give a slightly too small absolute value for the self-energy near μ (Ref. 10). While for the Anderson impurity model this behavior is not important for temperatures $T \gtrsim 0.1T_K$ (Ref. 10), the self-consistency process involved here naturally accumulates this deficiency, leading to the observed small discrepancies between QMC and NCA in the spectra and $\zeta^{-1}(T)$. Eventually the NCA breaks down completely for temperatures small compared to T_0. However, from our comparison one can conclude that the results produced by the NCA are reliable for $T/T_0 \gtrsim 1/5$.

For small U and/or far away from half filling the latter restriction makes the NCA obviously rather useless, because the low-temperature energy scale is usually of the order $O(1)$ here [see, for example, Fig. 3(d) with $\mu = 1.5$ and $\beta = 14.4$]. However, in the interesting region of large U and close to half filling the low-temperature scale T_0 is much smaller. In these cases the NCA provides a fast and consistent way to obtain information that is hard to access by other methods. For example, let us discuss the one-particle self-energies and the reentrance behavior found in the phase diagram at half filling (see Fig. 1).

The imaginary part of the one-particle self-energy is a quantity interesting in its own right since it provides valu-

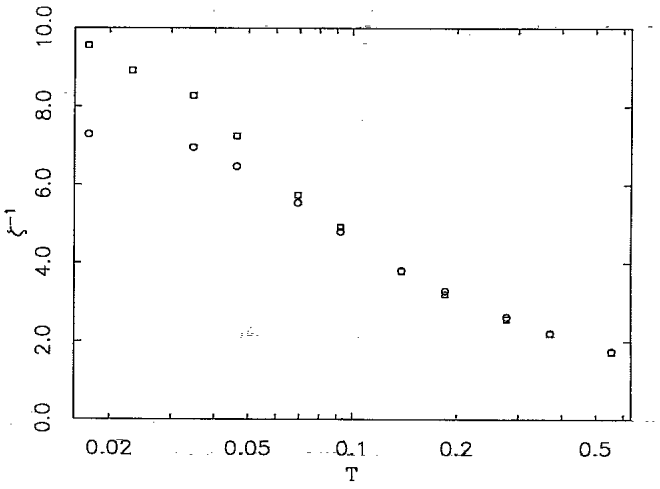

FIG. 4. Quasiparticle weight [see Eq. (6)] for $\mu = 1$, $U = 4$ as a function of temperature for QMC (circles) and NCA (squares). Note that the NCA starts to saturate to a slightly larger value but shows a renewed upturn for the lowest temperature. This must be attributed to a true failure of the approximations involved.

able information about the low-temperature behavior of the system. For a normal Fermi liquid when $T \to 0$, one expects $-\mathrm{Im}\Sigma(\omega+i\delta)$ to exhibit a parabolic minimum at μ with a curvature and temperature dependence that is characteristic of the effective mass of the quasiparticles in the system. A way to obtain this latter information has already been discussed with the definition of the quasiparticle weight equation (8). Figure 5 gives an impression of how the self-energy behaves for some parameter values, namely at half filling ($n_e = 1$) for two values of $U = 2,\ 4$ for a fixed temperature $\beta = 7.2$ in Fig. 5(a) and off half filling ($n_e \approx 0.94$) for a fixed $U = 4$ and two characteristic temperatures $\beta = 3.6,\ 28.8$ in Fig. 5(b). While for $U = 2$ [solid curve in Fig. 5(a)] and off-half filling [Fig. 5(b)] $|\mathrm{Im}\Sigma|$ obviously develops a nice parabolic minimum at μ, the behavior for $U = 4$ at half filling [dashed curve in Fig. 5(a)] is completely different. Here a sharp peak at μ appears separated by a (pseudo)gap from the continuum of particle-hole excitations. From general arguments[14] it follows that $-\mathrm{Im}\Sigma(\mu + i\delta) \approx 1/A(\mu)$ in this case. It is clear that one will never obtain a Fermi liquid with this type of self-energy[27]. Physically, this peak corresponds to an effective resonant scattering provided by the medium surrounding a given particle, thus localizing it by forming a bound state. It is nevertheless surprising to find such a structure when general phase-space arguments rather suggest that particle-hole scattering near μ has to vanish[28]. Thus an important question is whether this structure is stable or may be replaced by the usual minimum for $T \to 0$. This leads us directly to the reentrance behavior seen in Fig. 1.

To study this interesting behavior more closely we fix the Coulomb parameter at $U = 3.5$ and scan the temperature from above the MI crossover region ($T = 0.32$) down to $T = 0.002$. Obviously, such a low temperature cannot be reached with QMC for this value of U. The results are shown in Fig. 6. One nicely sees the opening of the pseudogap as the temperature is lowered. Eventually, this pseudogap is destroyed by a very narrow resonance at μ which also signals the onset of Fermi-liquid behavior. From the value of $A(\mu)$ we extrapolate to a low-temperature scale $T_0 \lesssim 1/400$. Thus, the Fermi liquid that eventually emerges has extremely large Fermi-liquid parameters. Another question is why such an Abrikosov-Suhl resonance can be built up from an insulator at all? Here we must keep in mind that we merely observe a pseudogap, i.e., the DOS around μ is never exactly zero and consequently will lead to a small but finite low-temperature scale T_0. Whether the Fermi-liquid phase will win depends entirely on the balance between the energy gain due to the delocalization of the particles in the narrow band at μ and the loss in correlation energy for the same reasons. It definitely seems more favorable for $3 < U < 4$ but we cannot decide from the data available whether the transition line will finally intercept the abscissa at a $U < \infty$ or not. We must stress at this point that this whole scenario is valid *if and only if* we have sufficient magnetic frustration to suppress or destroy the antiferromagnetic transition appearing in the phase diagram.

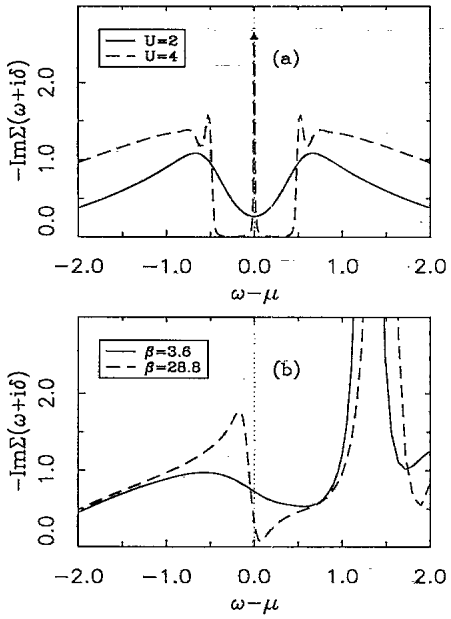

FIG. 5. Imaginary part of the self-energy for half filling and $U = 2, 4$ at a fixed temperature $\beta = 7.2$ (a) and $n_e \approx 0.94$ and $\beta = 3.6, 28.8$ for fixed $U = 4$ (b). The arrow at μ in $-\mathrm{Im}\Sigma(\omega+i\delta)$ for half filling and $U = 4$ in (a) indicates a very narrow peak with a height of the order $O(10^3)$.

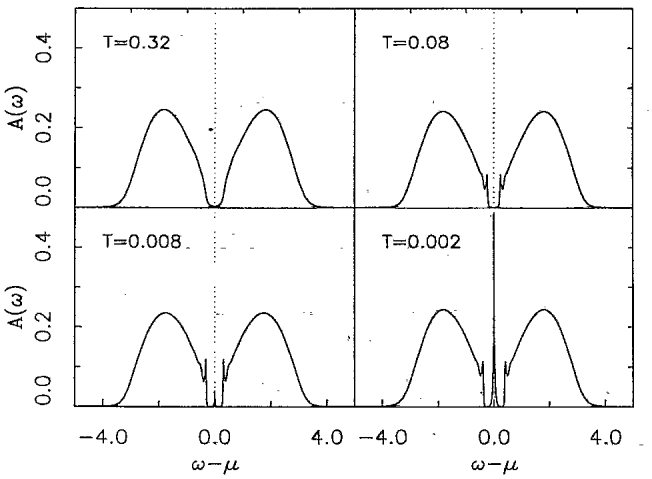

FIG. 6. DOS for the Hubbard model at half filling and $U = 3.5$ for different temperatures obtained with the NCA. The temperatures were chosen so that one cuts through the leftmost part of the insulating region in Fig. 1. Note the opening of the pseudogap when one lowers the temperature, which eventually is split by the ASR when one crosses the MI line again.

III. THERMODYNAMIC AND TRANSPORT PROPERTIES

The peculiar features of the single-particle DOS and self-energy discussed in the preceding section motivate a closer inspection of thermodynamic and transport properties of the Hubbard model (1) in the paramagnetic phase. Except for the one-dimensional model, a thor-

ough study of these quantities in the thermodynamic limit was not possible yet. Previous results from QMC simulations[29] are usually restricted to relatively small values of U or comparatively high temperatures. Since they are carried out on a finite lattice with a discrete energy spectrum, they probably will also miss the Kondo effect if it persists in three dimensions. The simplifications arising in $d = \infty$, however, make it possible to give closed expressions for several quantities, including the free energy, internal energy, and optical conductivity, which involve only the one-particle propagators in a simple way. We are thus in principle in a position to calculate these quantities exactly or, since we shall use the NCA to solve Eqs. (2) and (3), obtain at least a very good approximation for them.

Although the derivation of the expressions for those quantities is straightforward we will just state the final results and leave the mathematics to the Appendixes. To start with, the thermodynamic potential $\Omega(T)$ is given by[4]

$$\beta\Omega = N\beta\Omega_{\rm imp} - \sum_{\mathbf{k}} \mathrm{Tr}\,\ln\left(\frac{G_{ii}}{G_{\mathbf{k}}}\right) \quad . \tag{7}$$

Here, $\Omega_{\rm imp}$ is the local free-energy contribution from the effective Anderson impurity problem. Although, in principle, the knowledge of $\Omega(T)$ provides everything one needs, it is helpful to have an independent expression for the internal energy $E(T)$, too. The main reason is that thermodynamic quantities are usually obtained by differentiating $\Omega(T)$, which is a rather unpleasant task from a numerical point of view. In particular, the specific heat is a second derivative of Ω, but it is a first of $E(T)$. An expression for $E(T)$ is given by

$$E(T) = \tfrac{1}{2}\sum_{\mathbf{k}\sigma}\int d\omega\, f(\omega)\,(t_{\mathbf{k}} + \omega)\,A_{\mathbf{k}\sigma}(\omega) + \tfrac{1}{2}\mu N_e \quad . \tag{8}$$

The last quantity we want to study in this paper is the conductivity. We restrict ourselves to the $\mathbf{q} = \mathbf{0}$ component, because without coupling to elastic degrees of freedom we do not expect the model (1) to exhibit any incommensurate charge-density instability, i.e., the $\mathbf{q} = \mathbf{0}$ component will be the most important one. In this particular case, the limit $d \to \infty$ provides us with an extreme simplification, namely one can easily show (see e.g., Ref. 28 and the Appendixes) that the expression for $\sigma(\omega, T)$ reduces to

$$\sigma(\omega) = \pi \int d\omega' \int d\epsilon\, A_0(\epsilon) A(\epsilon, \omega') A(\epsilon, \omega' + \omega) \times \frac{f(\omega') - f(\omega' + \omega)}{\omega} \quad . \tag{9}$$

Note that for $\omega \to 0$ this is very similar to the result of Schweitzer and Czycholl[30], except that our result is written as energy integrals and thus avoids their explicit sum on lattice sites that is impossible to evaluate in $d \to \infty$.

Let us begin with a discussion of the properties of the model (1) at half filling. Due to numerical difficulties the NCA is currently not able to provide stable enough results in the interesting region just above the MI crossover line. We therefore have to concentrate on a value just below the critical one and we found it to be a convenient choice to use $U = 3$. As it turns out, the behavior found here is already close to what one may expect in the "insulating" region.

Before we turn to the actual thermodynamic properties, we first want to give with Fig. 7 an impression of the variation of the one-particle spectra with temperature. It is clear that the dip in the DOS at μ for higher temperatures is a poor replacement for the actual exponentially small DOS at larger values of U. However, together with the Abrikosov-Suhl resonance at low temperatures it gives a fairly good picture of the general temperature dependence of the DOS even for $U > U_c$. From it we may anticipate the behavior of the various thermodynamic and transport properties: Starting from high temperatures, one will encounter a temperature regime (e.g., $t^* > T \gg T_0$) where the DOS mainly consists of two separated bands. For the entropy, for example, this means that it will be rather flat with a value reflecting the degeneracy of the states in the lower band, i.e., $S \approx \ln 2$. At the same time the specific heat will decrease and become very small. If there were a true gap we would actually expect $C_V \sim \exp(-\beta\Delta_{\rm gap})$. The resistivity, on the other hand, will be large and increases with decreasing temperature, while the optical conductivity is governed by the charge excitations of energy U and shows no Drude peak.

Figure 8 displays the different thermodynamic quantities for the parameters under consideration as a function of temperature. In addition, we include for comparison some values of the internal energy $E(T)$ as obtained from QMC (circles). Again, QMC and NCA are found to be in good agreement. It is noteworthy that the internal energy becomes rather flat at $T \approx 1/5$. At the same time the entropy has a saddle point with a value of $S \approx \ln 2$,

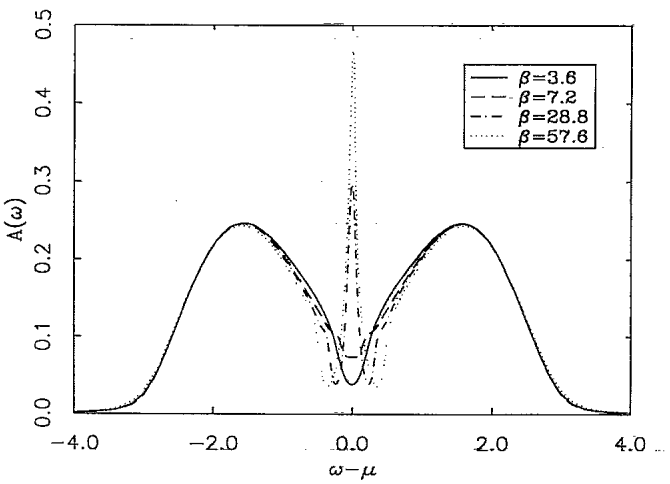

FIG. 7. Temperature dependence of the DOS for $U = 3$. Although there clearly is no gap in the spectrum, the overall temperature dependence is similar to the one expected for larger values of U: The dip in the DOS at μ for high T is replaced by a resonance at low T.

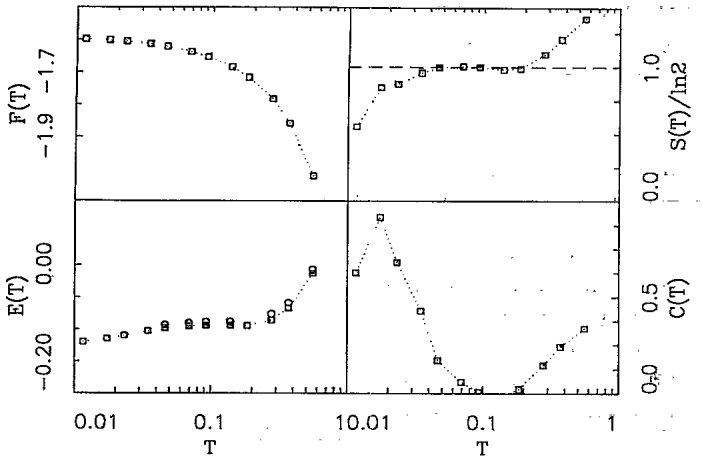

FIG. 8. Thermodynamic quantities for the Hubbard model at half filling with $U = 3$. Note the good agreement between QMC (circles) and the NCA results (squares) for the internal energy.

and the specific heat becomes small, as expected. The unphysical variation of $S(T)$ and $C(T)$ found in this interval must be attributed to numerical inaccuracy. In fact, by increasing the precision of the results we observed that, e.g., the nonmonotonic variation in $S(T)$ is reduced considerably while the value seems to approach $S \approx \ln 2$ with good accuracy. Also, the internal energy appears to be much more insensitive to numerical inaccuracies than the free energy.

When the temperature is further lowered, we see a decrease of $S(T)$ again, accompanied by a strong increase of $C(T)$, which eventually shows a maximum. This peak in $C(T)$ is a further fingerprint of the Kondo effect in this model. Unfortunately, a further decrease in temperature is not possible, since the NCA pathology becomes important for $T \lesssim 0.01$. From our experience this points towards a proper low-temperature energy scale of about $T_0 \approx 1/20$, which is also consistent with the position of the peak in $C(T)$ at $T \approx T_0/3$. At present one can only infer from the knowledge of the properties of heavy-fermion materials that $C(T) \sim T/T_0$ for temperatures below the maximum.

From these results one may easily extrapolate to the behavior of the system for $U > 3$. In fact, we mainly expect the extent of the flat region in $E(T)$ and $S(T)$ to become larger, namely it should last roughly until a possible crossover into the Kondo regime begins. Then one will find a very steep decrease of both quantities again. For values of U smaller than $U = 3$, on the other hand, the flat region will shrink and the slope of the decrease for lower temperatures will become smaller.

The resistivity for these parameter values as a function of temperature is shown in Fig. 9. Consistent with the DOS and the thermodynamics we first observe a semimetallic increase at high temperatures which goes through a maximum and then decreases for low temperatures. Since we expect the system to behave like a Fermi liquid at low temperatures, the resistivity should follow $\rho(T) = \rho_0 + a(T/T_0)^2$, where $\rho_0 = 0$, $T_0 \approx 1/20$, and $a = O(1)$. The calculated data generally follow this law when we also allow for a small intercept $\rho_0 \approx -5 \times 10^{-2}$ (see inset in Fig. 9). It is obvious that this negative intercept is a pure artifact and related to the pathology of the NCA: As discussed earlier, the approximations in the NCA tend to give a too small value of $\mathrm{Im}[\mathcal{G}^{\mathrm{NCA}}(\omega+i\delta)]^{-1}$ near μ. Since the self-energy is given by the difference between this quantity and the effective hybridization equation (3), one will eventually encounter a temperature where causality is violated and the results by the NCA become meaningless. For the present parameter values this happens for $T \lesssim 1/100$. It is clear that this breakdown will manifest itself strongest right at the minimum of $\mathrm{Im}\Sigma(\omega - i\delta)$, which happens to be always exactly at μ at half filling due to the particle-hole symmetry. Since the low-temperature resistivity, on the other hand, is approximately just given by $\mathrm{Im}\Sigma(-i\delta)$ (Ref. 31), this violation of causality produced by the NCA leads directly to the observed unphysical value of ρ_0.

The picture for half filling is completed by the optical conductivity in Fig. 10. As expected, the case $U = 3$ already gives an idea how the insulator will look: For high temperatures one finds a weak vestige of the Drude peak for $\omega \to 0$ which at first is suppressed when the temperature is lowered. Note, however, that we always maintain a finite value for $\sigma(0)$ consistent with the DOS in Fig. 7. At the same time the spectral weight of the charge excitation peak at $\omega = U$ increases. When we further lower the temperature, the situation reverses. A Drude peak at $\omega = 0$ builds up again (see inset in Fig. 10) and the spectral weight at $\omega = U$ is decreased. In addition, a shoulder emerges at $\omega \approx 1$. This feature must be ascribed to the additional excitations from the lower Hubbard band to the Abrikosov-Suhl resonance at μ. Note that the spectral weight associated with this additional resonance is rather small.

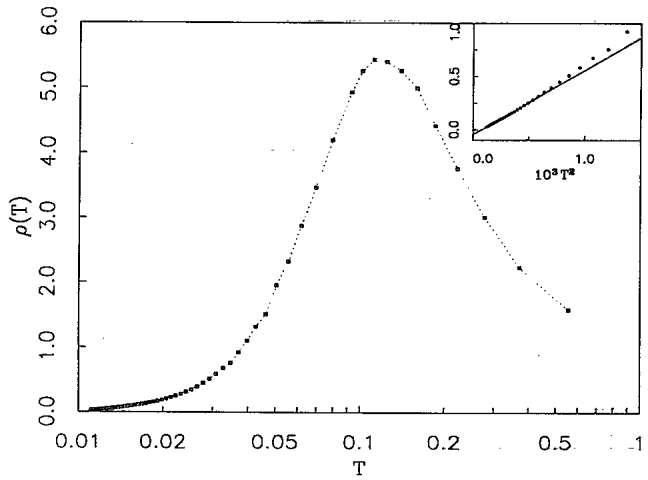

FIG. 9. Resistivity for the half-filled Hubbard model with $U = 3$ in units of $\left[\pi e^2 a t^{*2}/(2\hbar)\right]^{-1} \approx 100\ \mu\Omega\,\mathrm{cm}$. The inset shows the low-temperature data plotted vs T^2 together with a fit $\rho(T) = \rho_0 + a(T/T_0)^2$, where $a = O(1)$ and $T_0 \approx 0.05$. The appearance of an artificial intercept $\rho_0 < 0$ is directly related to the pathology of the NCA (see text). Interestingly, such a behavior is absent in the results off half filling (see Fig. 14).

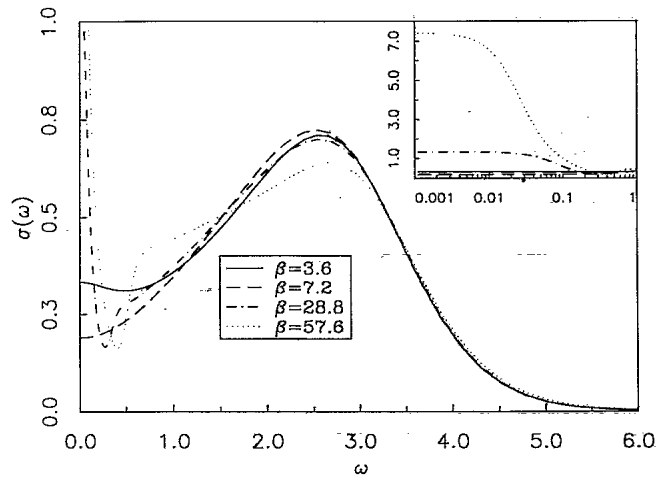

FIG. 10. Optical conductivity $\sigma(\omega)$ for the half-filled Hubbard model with $U = 3$ in units of $\pi e^2 a t^{*2}/(2\hbar)$. While the high-temperature variation is consistent with a semimetallic state, a conductor with a Drude peak at zero frequency is recovered when $T \to 0$. In the inset, the low-frequency results are shown on a semilogarithmic plot.

Let us finish the discussion of the half-filled case with a look at the typical behavior of the optical conductivity inside the insulator region in Fig. 1. Although the numerical problems prohibit a discussion of thermodynamic quantities here the results prove to be stable enough to allow the calculation of σ. Figure 11 shows our results for the DOS [Fig. 11(a)] and $\sigma(\omega)$ [Fig. 11(b)] for a value of $U = 6$ and temperatures $\beta = 1.44$ (solid curves) and $\beta = 28.8$ (dashed curves). The high-temperature result represents a point in the semimetallic portion of the phase diagram (Fig. 1) and still shows a small peak at $\omega = 0$ due to the thermally induced states in the gap here. This feature is, however, completely lost in the "insulating phase," where only the charge excitation peak at $\omega = U$ survives. We point out that the high-temperature results for $U = 3$ are indeed similar to the general behavior found here even though the larger DOS at μ of course leads to a finite value for $\sigma(0)$ there.

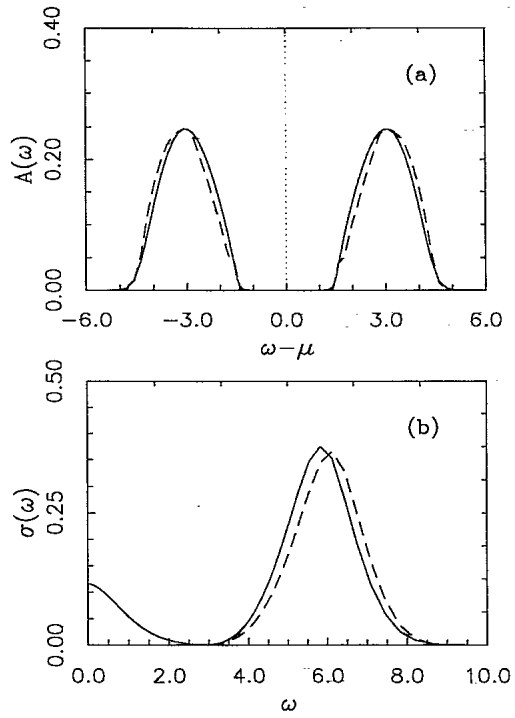

FIG. 11. DOS (a) and optical conductivity $\sigma(\omega)$ (b) for the half-filled Hubbard model with $U = 6$ for two temperatures $\beta = 1.44$ (solid line) and $\beta = 28.8$ (dashed line). The units are the same as in Fig. 10.

The situation of half filling is studied for the case $U = 4$ and $n_e = 0.97$. The variation of the DOS with temperature for these parameter values is collected in Fig. 12. Compared to the temperature dependence of $A(0)$ in Fig. 7, we observe a slower increase here, i.e., we have a somewhat smaller low-temperature scale T_0. From the value of $A(0; T = 1/28.8) \approx 2/\sqrt{\pi}$ we extrapolate to a $T_0 \lesssim 1/30$ for these parameter values. Although we are in principle able to trace the properties of the model (1) for a fixed electron density, it turns out that the obtainable numerical accuracy is not sufficient to get a reasonable result for the free energy. However, as already mentioned for the half-filled case, the internal energy $E(T)$ is much more well behaved and we shall concentrate on its behavior here. The results for the thermodynamics are collected in Fig. 13. The features found are actually very similar to the ones known from heavy-fermion physics, as expected: We observe a maximum in $C(T)$ at approximately $T_0/3$, where $T_0 \approx 1/30$ was read off the half height of the DOS in Fig. 12. Note that in contrast to half filling we do not have a pronounced flat region in $E(T)$ or $S(T)$ here. The values for the entropy in Fig. 13 were obtained by direct integration $S(T) = \int C(T)/T dT$. Taking into account the decreasing relative precision in $E(T)$ and the resulting large errors in $C(T)$ for lower temperatures we find, as expected, an entropy $S \approx \ln 2$ associated with the low-temperature peak in $C(T)$.

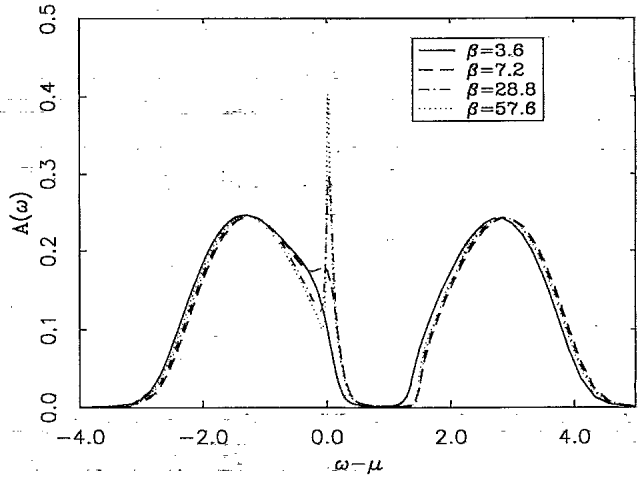

FIG. 12. Temperature dependence of the DOS for $U = 4$ and $n_e = 0.97$. Note that the increase of $A(0; T)$ with decreasing temperature is slower than for $U = 3$ and $n_e = 1$, indicating a smaller low-temperature scale T_0. From $A(0; T = 1/28.8) \approx 1/2\sqrt{\pi}$ we deduce a $T_0 \approx 1/30$ here.

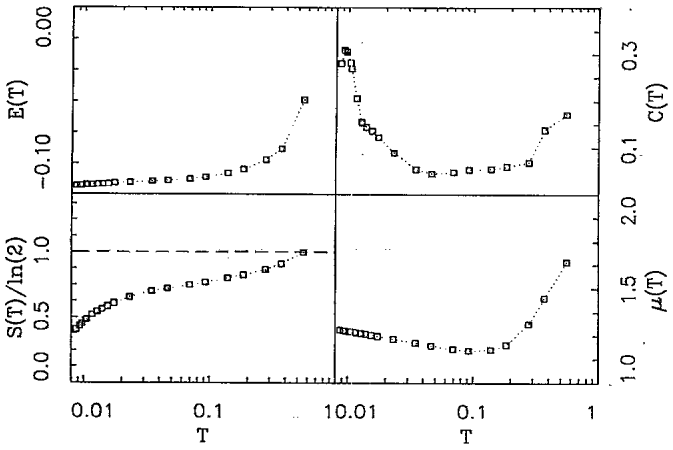

FIG. 13. Thermodynamic quantities for $U = 4$ and $n_e = 0.97$. The variation of μ with T is shown in the lower right picture. The results for the entropy were obtained from numerical integration of $C(T)/T$ (also see text).

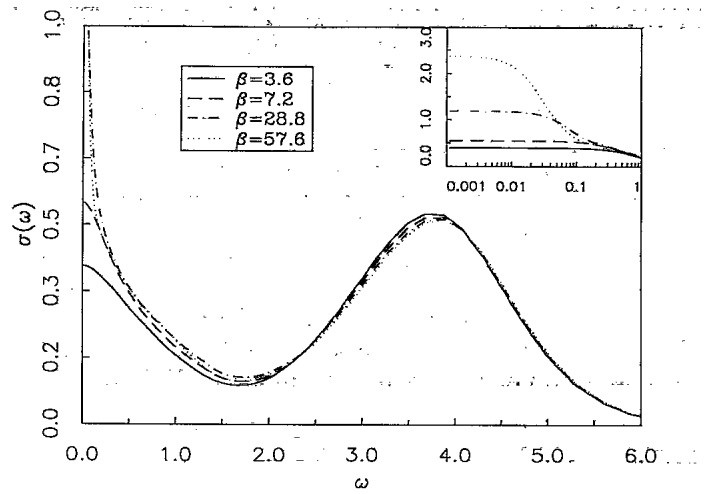

FIG. 15. Optical conductivity for $U = 4$ and $n_e = 0.97$ for some characteristic temperatures. Unlike for half filling we observe a Drude peak at $\omega = 0$ from the onset, i.e., the system is a metal for all temperatures. As in Fig. 10, the inset shows a semilogarithmic plot of the low-energy portion of the optical conductivity.

The resistivity in this case is shown in Fig. 14. As in the picture for half filling we observe an increase of $\rho(T)$ at high temperatures which eventually goes through a maximum. For low temperatures we find a power law $\rho(T) = a(T/T_0)^2$ with $T_0 \approx 30$ and $a = O(1)$ consistent with Fermi-liquid theory. This time we do not observe any unphysical behavior down to the lowest temperatures studied. This may be related to the fact that the slight shift of the minimum of $\mathrm{Im}\Sigma(\omega - i\delta)$ above μ sufficiently reduces the influence of the NCA pathology here.

It is noteworthy that for half filling and off-half filling the position of the maximum in $\rho(T)$ does not seem to be related to T_0 in a way similar to heavy-fermion systems. In fact, from the position of these maxima one would rather tend to rate the systems as weakly correlated. It is, however, important to remember that since the DOS at μ is strongly temperature dependent, the Kondo scale itself is a function of temperature.

Finally we present the optical conductivity for the parameter values $U = 4$ and $n_e = 0.97$ in Fig. 15 for some characteristic temperatures. The general structure is similar to half filling except that the Drude peak for $\omega \to 0$ continuously develops when the temperature is decreased. Also, the "Kondo" shoulder found in Fig. 10 is not visible here. Again, the weaker temperature dependence of $\sigma(\omega \to 0)$ points towards a smaller T_0 in this case.

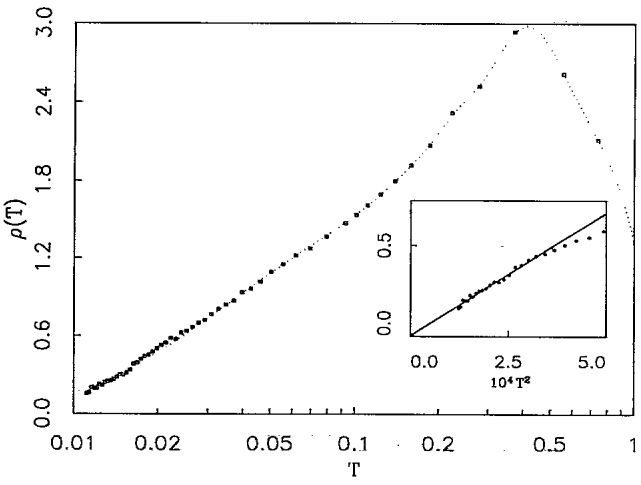

FIG. 14. Resistivity as a function of temperature for $U = 4$ and $n_e = 0.97$. For low temperatures we find $\rho(T) = a \cdot (T/T_0)^2$ (see inset) with $a = O(1)$. In contrast to half filling we do not observe any sizable deviation down to the lowest temperature points here. Note that the data are noisier than those for half filling. This must be attributed to the additional numerical inaccuracies due to tracing μ.

IV. SUMMARY

In this paper we have presented a detailed study of thermodynamic and transport properties of the Hubbard model on an infinite-dimensional hypercubic lattice. In contrast to the previous study[5,6] we did not take into account the antiferromagnetic ordering expected for this model with nearest-neighbor transfer, but concentrated on the paramagnetic case. The importance of such a study is motivated by the fact that inclusion of transfer beyond nearest neighbors will magnetically frustrate the system and thus depress the ordering. Besides, the effect of an antiferromagnetic transition on thermodynamic quantities like $S(T)$ and $C(T)$ is well known once their behavior in the paramagnetic regime is known.

The first part of this paper was devoted to a comparison between different approaches to the Hubbard model. As a reference point we used the essentially exact QMC method discussed extensively in Refs. 5 and 6. We found that a good description can be achieved by using the NCA to approximately solve the impurity Anderson model which enters the solution of (1) in infinite dimen-

sions. Using the NCA, the self-consistent set of equations can be solved very quickly which enabled us to present a variety of quantities as functions of temperatures for physically meaningful parameters. One of our main results is the interesting variation of the entropy and specific heat in the half-filled case. We believe that this behavior can be viewed as generic for the strongly correlated model. This conjecture was basically confirmed by the qualitative similarity between our results for half filling and $n = 0.97$.

Unfortunately, the NCA approach breaks down for too low temperatures due to an intrinsic violation of Fermi-liquid properties. However, our low-temperature results strongly suggest that a heavy-electron liquid builds up with a unique energy scale deductable from the variation of the various physical quantities. One thus can in principle adopt the well-developed phenomenology for these systems to extrapolate to a consistent low-temperature limit for the paramagnetic phase of the infinite-dimensional Hubbard model[32].

Together with our previous study, to the extent of our knowledge this represents the first consistent and reliable study of dynamic and thermodynamic properties of the $d > 1$ Hubbard model in the thermodynamic limit. Although the qualitative effects of finite-dimensional corrections are not well understood, we believe that many of the features found here will basically persist in at least $d = 3$.

ACKNOWLEDGMENTS

This research was supported by the National Science Foundation Grant No. DMR-88357341, the National Science Foundation Grant No. DMR-9107563, the Ohio State University Center of Materials Research, and the Ohio Supercomputing Center.

APPENDIX A: EXPRESSIONS FOR $\Omega(T)$ AND $E(T)$

In the following we will provide the derivation of the expressions for the free energy (9) and internal energy (10) for the Hubbard model in $d \to \infty$.

Let us start with the free energy. According to Baym[4,33] one can quite generally write the grand canonical potential as

$$\beta\Omega(\underline{\Sigma}) = \Phi(\underline{G}) - \mathrm{Tr}(\underline{\Sigma}\cdot\underline{G}) - \mathrm{Tr}\ln[(\underline{G}^0)^{-1} - \underline{\Sigma}], \quad \text{(A1)}$$

where shorthand matrix notations

$$(\underline{G})_{ij;nm} = G_{ij}(i\omega_n, i\omega_m)$$

and

$$(\underline{\Sigma})_{ij;nm} = \Sigma_{ij}(i\omega_n, i\omega_m)$$

were introduced. The functional Φ is defined via the perturbation expansion of $\underline{\Sigma}$ in terms of $\underline{G}$ by the property

$$\frac{\delta\Phi}{\delta\underline{G}} = \underline{\Sigma}\ . \quad \text{(A2)}$$

For $d \to \infty$ we know that $\underline{\Sigma}(z) \equiv \Sigma(z)\underline{1}$ and its perturbation expansion involves only the local component of $\underline{G}$, $G_{ii}(z)$. This implies that $\Phi(\underline{G}) = \Phi(\{G_{ii}\}) = N\Phi_{\mathrm{imp}}(G_{ii})$ (Refs. 2 and 4) and finally

$$\begin{aligned}\beta\Omega(T) &= N\Phi_{\mathrm{imp}}(G_{ii}) - N\,\mathrm{Tr}(\Sigma G_{ii}) - N\,\mathrm{Tr}\,\ln(G_{ii}^{-1}) \\ &\quad - \sum_{\mathbf{k}} \mathrm{Tr}\,\ln\left(\frac{G_{ii}}{G_{\mathbf{k}}}\right) \\ &= N\beta\Omega_{\mathrm{imp}} - \sum_{\mathbf{k}} \mathrm{Tr}\ln\left(\frac{G_{ii}}{G_{\mathbf{k}}}\right)\ . \end{aligned} \quad \text{(A3)}$$

Here, Ω_{imp} is the local free-energy contribution from the effective Anderson impurity problem for a given Σ (Ref. 4).

For the derivation of $E(T)$ we first note that from $\Omega = E - TS - \mu N$ one obtains for fixed particle number $E = \partial(\beta\Omega)/\partial\beta + \mu N + \beta\partial\mu/\partial\beta N_e$. With $\Omega = -\beta^{-1}\ln Z$ this leads to the relation $E(T) = \langle H\rangle + \mu N_e$. Note that this unusual form arises because our definition of the Hubbard Hamiltonian (1) absorbs the term $-\mu N$. In order to calculate the expectation value, let us evaluate the following commutator[34]:

$$\begin{aligned}\sum_{i\sigma} c_{i\sigma}^\dagger[c_{i\sigma}, H] &= \sum_{i,l,j,\sigma} t_{jl}(c_{i\sigma}^\dagger[c_{i\sigma}, c_{l\sigma}^\dagger c_{j\sigma}] + c_{i\sigma}^\dagger[c_{i\sigma}, c_{j\sigma}^\dagger c_{l\sigma}]) - \mu\sum_{ij\sigma} c_{i\sigma}^\dagger[c_{i\sigma}, n_{j\sigma}] + \sum_{i,l,\sigma} c_{i\sigma}^\dagger[c_{i\sigma}, n_{l\uparrow}n_{l\downarrow}] \\ &= H_{\mathrm{kin}} - \mu N + 2U = 2H - H_{\mathrm{kin}} + \mu N\ . \end{aligned} \quad \text{(A4)}$$

That means for $\langle H\rangle$

$$\begin{aligned}\langle H\rangle &= \frac{1}{2}\left\langle H_{\mathrm{kin}} + \sum_{i\sigma} c_{i\sigma}^\dagger[c_{i\sigma}, H]\right\rangle - \tfrac{1}{2}\mu N_e + \tfrac{1}{2}\sum_{\mathbf{k}\sigma} t_{\mathbf{k}}\langle c_{\mathbf{k}\sigma}^\dagger c_{\mathbf{k}\sigma}\rangle + \tfrac{1}{2}\sum_{i\sigma}\langle c_{i\sigma}^\dagger[c_{i\sigma}, H]\rangle - \tfrac{1}{2}\mu N_e \\ &= \tfrac{1}{2}\sum_{\mathbf{k}\sigma} t_{\mathbf{k}} G_{\mathbf{k}\sigma}(-\delta) + \tfrac{1}{2}\sum_{i\sigma} G_{[c_{i\sigma},H],c_{i\sigma}^\dagger}(-\delta) - \tfrac{1}{2}\mu N_e \\ &= \frac{1}{2\beta}\sum_{i\omega_n}\left(\sum_{\mathbf{k}\sigma} t_{\mathbf{k}} G_{\mathbf{k}\sigma}(i\omega_n) + \sum_{i\sigma} G_{[c_{i\sigma},H],c_{i\sigma}^\dagger}(i\omega_n)\right) e^{i\omega_n\delta} - \tfrac{1}{2}\mu N_e. \end{aligned} \quad \text{(A5)}$$

With the equation of motion

$$zG_{ii}(z) = 1 + G_{[c_{i\sigma},H],c^{\dagger}_{i\sigma}}(z) \tag{A6}$$

and using translational invariance, i.e., $G_{ii}(z) = \frac{1}{N}\sum G_{\mathbf{k}\sigma}(z)$, one arrives at

$$E(T) = \frac{1}{2\beta}\sum_{i\omega_n}\sum_{\mathbf{k}\sigma}\left[t_{\mathbf{k}}G_{\mathbf{k}\sigma}(i\omega_n) + i\omega_n G_{\mathbf{k}\sigma}(i\omega_n) - 1\right]e^{i\omega_n\delta} + \tfrac{1}{2}\mu N_e \quad . \tag{A7}$$

Now,

$$\frac{1}{\beta}\sum_{i\omega_n} G_{\mathbf{k}\sigma}(i\omega_n) = \int d\omega f(\omega) A_{\mathbf{k}\sigma}(\omega)$$

and with $\int d\omega A_{\mathbf{k}\sigma}(\omega) = 1$

$$\begin{aligned}\frac{1}{\beta}\sum_{i\omega_n}[i\omega_n G_{\mathbf{k}\sigma}(i\omega_n) - 1]e^{i\omega_n\delta} &= \frac{1}{\beta}\sum_{i\omega_n}\int d\omega\, A_{\mathbf{k}\sigma}(\omega)\left(\frac{i\omega_n}{i\omega_n - \omega} - 1\right)e^{i\omega_n\delta} \\ &= \frac{1}{\beta}\sum_{i\omega_n}\int d\omega\, A_{\mathbf{k}\sigma}(\omega)\frac{\omega}{i\omega_n - \omega}e^{i\omega_n\delta} \\ &= \int d\omega\, \omega f(\omega) A_{\mathbf{k}\sigma}(\omega)\end{aligned}$$

the final equation reads

$$E(T) = \tfrac{1}{2}\sum_{\mathbf{k}\sigma}\int d\omega\, f(\omega)\,(t_{\mathbf{k}} + \omega)\, A_{\mathbf{k}\sigma}(\omega) + \tfrac{1}{2}\mu N_e \quad . \tag{A8}$$

APPENDIX B: OPTICAL CONDUCTIVITY

In general, the conductivity tensor is expressed via the current-current susceptibility as

$$\begin{aligned}\sigma_{kl}(\omega) &= -\frac{1}{N}\mathrm{Re}\left\{\frac{1}{i\omega}\chi_{j_l,j_k}(\omega + i\delta)\right\} \\ &= \frac{1}{N}\mathrm{Re}\left\{\frac{1}{i\omega}\langle\langle j_l|j_k\rangle\rangle(\omega + i\delta)\right\} \\ &\equiv \mathrm{Re}\tilde{\sigma}_{kl}(\omega + i\delta) \quad .\end{aligned} \tag{B1}$$

For the simple cubic lattice under consideration, the tensor is proportional to the unit tensor, i.e.,

$$d\tilde{\sigma}(z) = \frac{1}{N}\frac{1}{iz}\sum_{l}\langle\langle j_l|j_l\rangle\rangle(z)\,. \tag{B2}$$

Further, the current operator for the Hubbard model (1) is given by ($e = \hbar = 1$)

$$\mathbf{j} = \sum_{\mathbf{k}\sigma}\mathbf{v}_{\mathbf{k}} n_{\mathbf{k}\sigma}, \tag{B3}$$

where the group velocity or the particles is defined via $\mathbf{v}_{\mathbf{k}} = \nabla t_{\mathbf{k}}$. This leads to

$$d\tilde{\sigma}(z) = \frac{1}{iz}\frac{1}{N}\sum_{\mathbf{k},\mathbf{k}',\sigma}\sum_{l} v_{k_l} v_{k'_l}\langle\langle n_{\mathbf{k}\sigma}|n_{\mathbf{k}'\sigma}\rangle\rangle(z) \quad . \tag{B4}$$

This expression has the perturbation expansion shown in Fig. 16. One important implication of the limit $d \to \infty$ is that the irreducible vertex $\Gamma(i\omega_n, i\omega_m; i\nu)$ in Fig. 16 has to be purely local[3]. This means that the $\mathbf{k}$ summations in the second part of Fig. 16 can be performed independently and thus these vertex corrections vanish, because $\mathbf{v}_{\mathbf{k}}$ has a different parity than $t_{\mathbf{k}}$ (Ref. 35). This means that only the simple bubble survives and we are left with (the lattice constant to be taken unity)

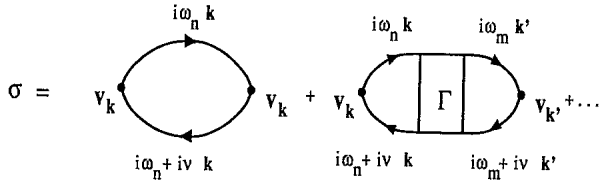

FIG. 16. First two contributions to the perturbation expansion for the conductivity, Eq. (23). Note that the irreducible vertex part $\Gamma(i\omega_n, i\omega_m; i\nu)$ in the second diagram is purely local, i.e., the different $\mathbf{k}$ vectors appearing on both sides can be summed over independently. Since $\mathbf{v}_{\mathbf{k}}$ has a different parity than $t_{\mathbf{k}}$, this contribution necessarily vanishes and so do all higher-order vertex corrections (Ref. 35).

$$\tilde{\sigma}(i\nu) = \frac{1}{\nu}\frac{1}{N\beta}\sum_{\mathbf{k}\sigma,\omega_n}\sum_{l} v_{kl}^2 G_{\mathbf{k}\sigma}(i\omega_n)G_{\mathbf{k}\sigma}(i\omega_n+i\nu) = \frac{1}{\nu}\frac{1}{N\beta}\sum_{\mathbf{k}\sigma,\omega_n}\sum_{l} 4t^2\sin^2(k_l)G_{\mathbf{k}\sigma}(i\omega_n)G_{\mathbf{k}\sigma}(i\omega_n+i\nu) \tag{B5}$$

for nearest-neighbor transfer.

The problem left is to evaluate the sum

$$\tilde{\rho}_0(\epsilon) = \frac{1}{N}\sum_{\mathbf{k}}\sum_{l}\sin^2(k_l)\delta(\epsilon - t_{\mathbf{k}}). \tag{B6}$$

For this purpose, we use the method applied by Müller-Hartmann[3] and study the Fourier transform of (B6),

$$\begin{aligned}\Psi_d(s) = \int \tilde{\rho}_0(\epsilon)e^{is\epsilon}d\epsilon = \frac{1}{N}\sum_{\mathbf{k}}\sum_{l}\sin^2(k_l)e^{ist_{\mathbf{k}}} &= d\left[\int_{-\pi}^{\pi} e^{-2ist\cos k}\frac{dk}{2\pi}\right]^{d-1}\left[\int_{-\pi}^{\pi}\sin^2 k e^{-2ist\cos k}\frac{dk}{2\pi}\right] \\ &= \frac{d}{2}\left[J_0(2st)\right]^d + \frac{d}{2}\left[J_0(2st)\right]^{d-1}J_2(2st)\ ,\end{aligned} \tag{B7}$$

where $J_\nu(z)$ are Bessel functions. Noting that $A_0(\epsilon) = \int ds\, e^{-is\epsilon}\left[J_0(2st)\right]^d$, we find

$$\frac{1}{N}\sum_{\mathbf{k}}\sum_{l}\sin^2(k_l)\delta(\epsilon - t_{\mathbf{k}}) = \frac{d}{2}\left(\rho_0(\epsilon) + \int_{-\infty}^{\infty} ds\, e^{-is\epsilon}\left[J_0(2st)\right]^{d-1}J_2(2st)\right)\ . \tag{B8}$$

This relation is valid for a simple cubic lattice and nearest-neighbor transfer in any dimension. For the current purpose we are only interested in the limit $d \to \infty$, where one can achieve a further substantial simplification. Noting that $2t \sim 1/\sqrt{d} \ll 1$ we may approximate $J_2(2st) \approx s^2t^2$ for large d and find for the last term in (B8)

$$\int ds\, e^{-is\epsilon}\left[J_0(2st)\right]^{d-1}J_2(2st) \approx t^2\int ds\, s^2 e^{-is\epsilon}\left[J_0(2st)\right]^d = -t^2\frac{d^2A_0(\epsilon)}{d\epsilon^2}\ . \tag{B9}$$

Since $t^2 \sim 1/d$ this term is negligible in the limit $d \to \infty$, i.e., $\tilde{\rho}_0(\epsilon) = d\rho_0(\epsilon)/2$ and finally

$$\tilde{\sigma}(i\nu) = \frac{1}{\nu}\frac{1}{\beta}\sum_{\omega_n}\int d\epsilon\, A_0(\epsilon)G(\epsilon,i\omega_n)G(\epsilon,i\omega_n+i\nu) = \frac{1}{\nu}\int d\epsilon\, d\omega\, d\omega' A_0(\epsilon)A(\epsilon,\omega)A(\epsilon,\omega')\frac{f(\omega)-f(\omega')}{\omega-\omega'+i\nu}\ . \tag{B10}$$

Taking the real part of the analytic continuation of Eq. (B10) leads to our final result for the optical conductivity

$$\sigma(\omega) = \pi\int d\omega'\int d\epsilon\, A_0(\epsilon)A(\epsilon,\omega')A(\epsilon,\omega'+\omega)\frac{f(\omega')-f(\omega'+\omega)}{\omega}\ . \tag{B11}$$

When we collect the missing constants we find for the unit of the conductivity

$$\sigma_0 = \frac{\pi e^2a^2t^{*2}}{2\hbar}\frac{N}{\mathrm{Vol}} \approx 10^{-2}\cdots 10^{-3}\,(\mu\Omega\,\mathrm{cm})^{-1}\ ,$$

for $t^* \approx 1$ eV and $a = O(a_0)$.

[1] W. Metzner and D. Vollhardt, Phys. Rev. Lett. **62**, 324 (1989).

[2] U. Brandt and Ch. Mielsch, Z. Phys. B **75**, 365 (1989); **79**, 295 (1990).

[3] E. Müller-Hartmann, Z. Phys. B **74**, 507 (1989).

[4] V. Janiš and D. Vollhardt (unpublished).

[5] M. Jarrell, Phys. Rev. Lett. **69**, 168 (1992). See also the subsequent work of M. Rosenberg, X. Zhang, and G. Kotliar (unpublished); A. Georges and W. Krauth (unpublished).

[6] M. Jarrell and Th. Pruschke, Z. Phys. (to be published).

[7] A. Georges and G. Kotliar, Phys. Rev. B **45**, 6479 (1992).

[8] J. Hubbard, Proc. R. Soc. London Ser. A **276**, 238 (1963); M.C. Gutzwiller, Phys. Rev. Lett. **10**, 159 (1063); J. Kanamori, Prog. Theor. Phys. **30**, 257 (1963).

[9] H.R. Krishnamurthy, J.W. Wilkins, and K.G. Wilson, Phys. Rev. B **21**, 1003 (1980).

[10] N.E. Bickers, D.L. Cox, and J.W. Wilkins, Phys. Rev. B **36**, 2036 (1987).

[11] Th. Pruschke and N. Grewe, Z. Phys. B **74**, 439 (1989).

[12] V. Zlatić and B. Horvatić, Phys. Rev. B **28**, 6904 (1983).

[13] K. Yamada and K. Yosida, *Theory of Heavy Fermions and Valence Fluctuations*, edited by T. Kasuya and T. Saso (Springer, Berlin, 1985).

[14] E. Müller-Hartmann, Z. Phys. B **76**, 211 (1989).

[15] B. Menge and E. Müller-Hartmann, Z. Phys. B **82**, 237 (1991).

[16] V. Zlatić, B. Horvatić, and D. Sokcevic, Z. Phys. B **59**, 151 (1985).

[17]H. Keiter and J.C. Kimball, Int. J. Magnetism **1**, 233 (1971).
[18]N. Grewe, Z. Phys. B **53**, 271 (1983); Y. Kuramoto, *ibid.* **53**, 73 (1983).
[19]E. Müller-Hartmann, Z. Phys. B **57**, 281 (1984).
[20]N. Grewe and H. Keiter, Phys. Rev. B **24**, 4420 (1981).
[21]Y. Kuramoto, *Theory of Heavy Fermions and Valence Fluctuations*, edited by T. Kasuya and T. Saso (Springer, Berlin, 1985).
[22]N. Grewe, Z. Phys. B **67**, 323 (1987).
[23]N. Grewe, Th. Pruschke, and H. Keiter, Z. Phys. B **71**, 75 (1988).
[24]N. Grewe and Th. Pruschke, Solid State Commun. **67**, 205 (1988).
[25]Th. Pruschke, Z. Phys. B **81**, 319 (1990).
[26]See, for example, D.W. Hess and J.W. Serene, J. Phys. Chem. Solids **52**, 1185 (1991).
[27]This particular behavior also explains why any finite-order perturbation theory in U will have serious problems to recover this result, since these theories produce Fermi-liquid behavior by construction (Ref. 28).
[28]J.M. Luttinger and J.C. Ward, Phys. Rev. **118**, 1417 (1960).
[29]See, for example, J.E. Hirsch, Phys. Rev. B **35**, 1851 (1987); R.T. Scalettar *et al.*, *ibid.* **39**, 4711 (1989).
[30]H. Schweitzer and G. Czycholl, Phys. Rev. Lett. **67**, 3724 (1991).
[31]K. Murata, Ph.D. thesis, Cornell University, 1970.
[32]F.J. Ohkawa, J. Phys. Soc. Jpn. **61**, 1615 (1992).
[33]G. Baym, Phys. Rev. **127**, 836 (1962).
[34]This technique was pointed out to us by N. Grewe.
[35]A. Khurana, Phys. Rev. Lett. **64**, 1990 (1990).